SolarPACES 2024, 30th International Conference on Concentrating Solar Power, Thermal, and Chemical Energy Systems

Analysis and Simulation of CSP and Hybridized Systems

https://doi.org/10.52825/solarpaces.v3i.2454

Published: 17 Sep. 2025

Model Sensitivity Analysis of Lifetime Predictions for Generation 3 Particle-sCO_2 Heat Exchangers

Chris Bowen[1,*] and Matthew Sandlin[1]

[1]Concentrating Solar Technologies, Sandia National Laboratories

*Correspondence: Chris Bowen, cpbowen@sandia.gov

Abstract. A sensitivity analysis is performed to determine which variables play a first order role in determining the lifetime of particle-sCO_2 heat exchangers. A symmetric half-plate geometry based on a hypothetical 16.7 MW commercial scale particle-sCO_2 diffusion bonded IN617 heat exchanger is studied. A reduced-order modelling approach is presented and the steady-state and transient thermal and mechanical performances under nominal Generation 3 concentrated solar power operating conditions are compared against the fully featured model. The defeatured model shows the ability to accurately predict the thermal performance and mechanical lifetime at a fraction of the computational cost, making it a viable option for analysing commercial scale systems. Seven of the model input variables are then parameterized using a Latin Hypercube Sampling method and up to 128 different realizations are simulated. The transient stress results are linearized along stress classification lines in the header ports and used to predict the number of cycles to failure due to fatigue and creep. Sobol indices are generated to relate the cycles to failure to the independent variables studied. The results show that the uncertainty in the creep cycles to rupture data dominates the variation in lifetime predictions.

Keywords: Particle-Based CSP, Particle Heat Exchangers, Thermomechanical Modelling

1. Introduction

Generation 3 (Gen3) concentrating solar power/thermal (CSP/CST) technologies utilize solid particles as a heat transfer and thermal energy storage (TES) medium. While particle-based CSP/CST technologies have been identified as the most promising candidate to achieve levelized cost of electricity (LCOE) and heat (LCOH) targets of \$0.05/kWh and \$0.02/kW_{th}, respectively, this is highly contingent upon meeting the targeted mechanical lifetimes of the system's critical components. The particle-to-supercritical CO_2 (sCO_2) heat exchanger for example requires a minimum lifetime of 10,000 hours or 1,000 thermal cycles to achieve the Gen3 particle plot plant (G3P3) cost targets. While maximizing the area-to-volume ratio of the heat exchanger is desirable for maximizing thermal duty and minimizing material cost, uncertainty in mechanical durability necessitates more conservative, larger designs. This conservatism incurs additional cost that can be mitigated with a combination of high fidelity thermomechanical modeling and fatigue and creep testing relevant to diffusion bonded printed circuit heat exchangers. This work presents a simplified approach to predicting the transient stress fields during a nominal Gen3 operating cycle that can be applied to commercial scale designs. The primary loading, fatigue, and creep damage are evaluated using wrought material data, and a sensitivity study is performed to determine how uncertainty in material properties and in creep-fatigue failure data impact lifetime predictions. Understanding which variables have a first order

effect will inform future experimental efforts to characterize diffusion bonded material behavior under Gen3 conditions.

2. Model Setup and Simplified Approach Evaluation

The mesh sizes of commercial scale heat exchangers with complex microchannel networks present computational limitations. Even for the simplest continuum-based models where a relatively coarse mesh can be applied to the particle domain, a single Gen3 scale plate with fully featured channels will have over one hundred million elements. In this study a fully featured and defeatured model of shell-and-plate moving packed-bed counterflow heat exchanger for a 16.7 MW commercial scale design at Gen3 operating conditions are compared. The full design was provided by Vacuum Process Engineering and consists of 594 diffusion bonded plates. A single half-plate geometry is generated, which under nominal steady-state operation should have a thermal duty of approximately 14kW. The full geometry is depicted in Fig.1 where the plate is made transparent to show the advective bar lines that run through the center of the channels. The particle region is shown in solid red.

The model setup follows the approach detailed by Bowen and Albrecht [1] where the particle flow is modelled as a slip-walled continuum with temperature dependent fluid-thermal properties of Carbo HSP 40/70 particles with a void fraction of 0.45. This continuum-based Eulerian treatment, while simplistic, is much less complex and more efficient than multiphase or high-fidelity Discrete Element Method granular models. The heat flux at the particle-plate interface is handled using a contact interface with a prescribed gap conductance. The sCO_2 flow is approximated using 1D advective bars that require no fluid mesh but coupled to the surrounding walls using predefined Nusselt number correlations [2]. A standard Gnielinski [3] correlation was applied for turbulent flow coupling in this study. Modelling the sCO_2 fluid with adequate near-wall mesh resolution to accurately capture the wall heat flux quickly runs the overall conjugate model element count into the billions. This is computationally impractical for parametric evaluations or optimization studies. The full system steady design conditions are

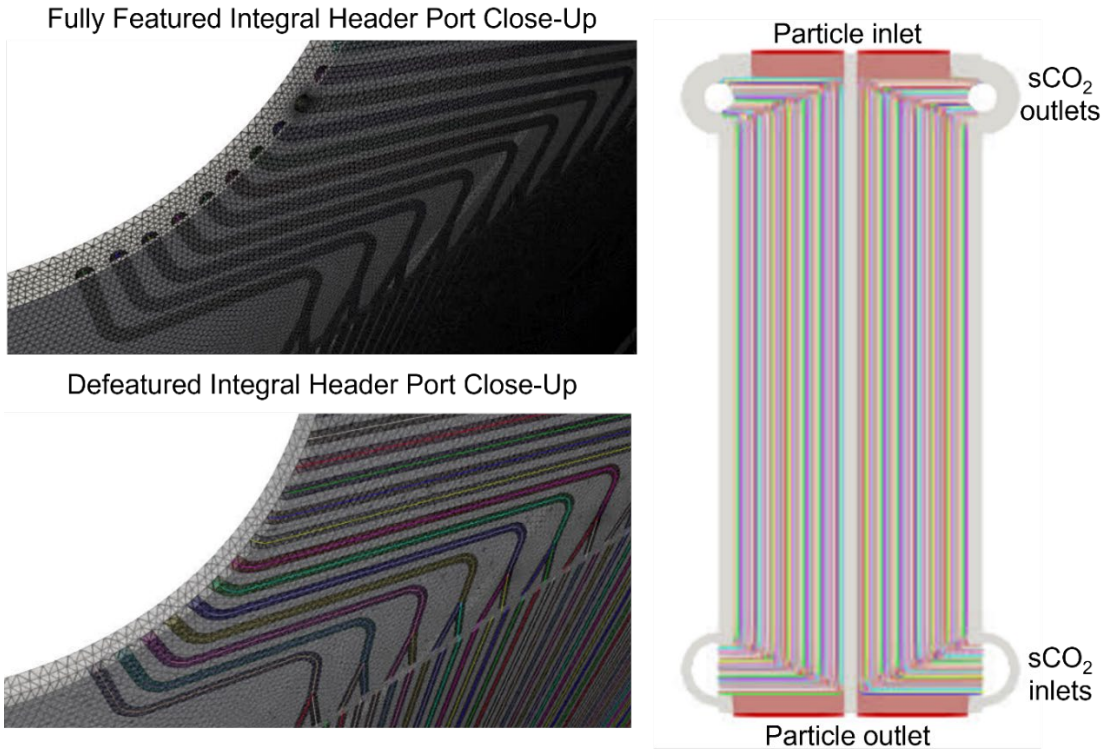

Figure 1. *Fully featured particle-sCO2 half-plate heat exchanger model (right) and close up of outlet integral header port showing mesh and advective bars centered in channels (left)*

provided in Table 1. The inlet mass flow rates to the particle region and sCO_2 advective bars are derived by dividing the system flow rate by the number of half-plates in the system, assuming particle and sCO_2 flow uniformity. The channel layout consists of 5 regions, each with a unique number of channels and with a horizontal mixing channel to redistribute the flow (and heat) as equally as possible into the next region. The inlet temperatures prescribed to the advective bars downstream are determined from a distance weighted averaging approach of the nearest upstream channels, which was found to conserve energy within 1% despite being a simplification. The steady state thermal and transient simulations in this work are performed in Sandia's native FEA multiphysics suite SIERRA Aria [4]. Mass and energy balances are monitored to assure steady conditions are achieved where appropriate. The thermomechanical simulations are performed in the SIERRA Arpeggio code [5]. The mechanical solver imports the thermal solution and uses a temperature versus mechanical strain function for Inconel® alloy 617 (IN617) to calculate thermal strains and stresses. The procedure is one-way coupled, and the mechanical deformation has no impact on the thermal solver. A pressure boundary condition of 25 MPa is applied to the inner surfaces of the microchannels and integral header ports to capture the primary stress contribution.

Table 1. *Commercial full system particle-sCO_2 heat exchanger design operating conditions*

Variable	Value
Particle flow rate	94.67 kg/s
Particle inlet temperature	775 °C
sCO_2 flow rate	87.84 kg/s
sCO_2 inlet temperature	565 °C
sCO_2 pressure	25 MPa

The defeatured version of the model is developed to reduce the overall mesh count. To accomplish this, the microchannels throughout the heat exchanger are filled with solid material. The removal of the microchannels in the header ports causes some local peak stresses to be ignored, however it is expected that in operation those stresses would relax closer to the local mean values due to creep. To couple the sCO_2 advective bar flow networks to the plate in the now solid core region, the plate was split in two down the centerline where the channels previously existed. 2D channel surfaces with width equal to the channel diameter were imprinted on each of the contacting surfaces as shown in the bottom close-up in Fig. 1. This provided a reference surface for each advective bar to couple to. A contact interface is then imposed on the remaining area of the split plates to match the heat flux between them. The overall mesh count was reduced from 72.7 million to 16.4 million by applying this defeaturing.

The steady state temperature and stress fields are compared between the fully featured and defeatured models in Fig.2 and show close qualitative agreement. The thermal duty of the fully featured version is 15kW, which is 7% higher than the design requirement per plate. The defeaturing of the model only results in a 1.3% reduction in the prediction of the steady thermal duty. The mechanical damage leading to eventual failure is assumed to occur in the header ports where the highest stresses occur. Figure 3 compares the linearized stress values of the steady state solutions along one of the four labelled stress classification lines (SCLs) for both the inlet and outlet headers. Stress linearization is a method of converting raw stress components into equivalent constant membrane and varying linear components along a predefined integration line. This allows for ASME Boiler and Pressure Vessel Code (BPVC) standards to be applied for design analysis. Figure 3 only shows the linearized results for two of the four SCLs on the inlet and outlet but illustrates that the linearized results are approximately equal between the featured and defeatured approaches. At steady state operation then, the defeatured model should be able to predict plastic failure that may occur. The divergence between the von Mises distribution (green) and linearized distribution (black) at the outer radius of the north and south SCLs is due to the peak corner stresses. Those stresses will relax in practice, but the lack of a creep model prevents that physics from being captured. The allowable stress (Sa) limits used to determine if the steady solutions are viable, as described in the

next section, are also plotted. Since the heat exchanger spends the majority of a 24-hour cycle at or near steady operating conditions, this approach should also give a reasonable creep damage approximation. The fatigue damage due to the transient behavior was found to be a negligible contributor over reasonable ramp rates (5-20 °C/min), so potential differences in the ramp up/down behavior between the models will have a negligible effect on the lifetime predictions. The domain was further simplified by splitting it down the centerline and applying symmetry boundaries, cutting the mesh down to 8.2 million. The fully featured steady solution took 6.5 hours to run on 360 parallel processors, while the defeatured symmetric version completed in only 1.5 hours on 256 processors.

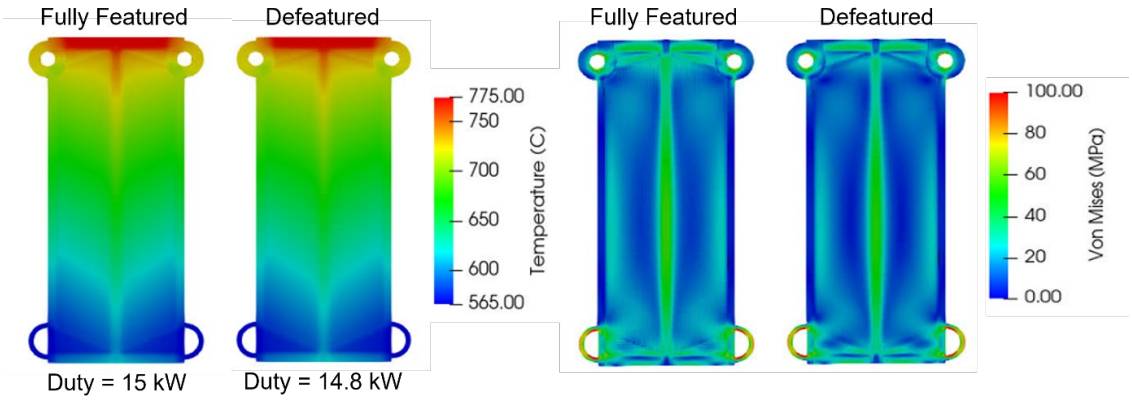

Figure 2. *Comparison of steady state temperature and von Mises stress distributions between featured and defeatured models*

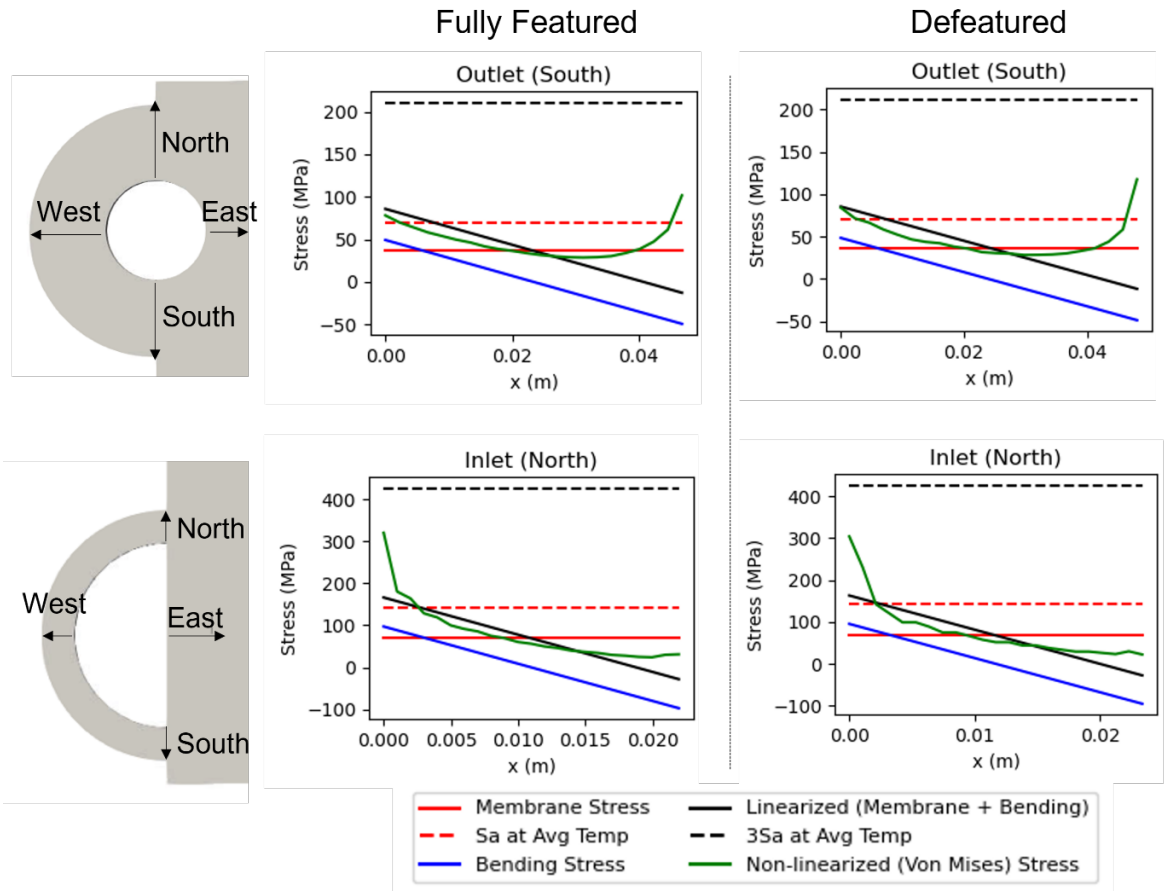

Figure 3. *Comparison of fully featured and defeatured steady state linearized stresses along stress classification lines at outlet and inlet headers*

0th International Conference on

3. Lifetime Prediction Procedure

The thermomechanical model workflow was setup to generally follow the recommendations for high temperature CSP component design developed by Argonne National Labs [6]. The first step is a primary load check to ensure the heat exchanger will not fail under steady operation. The steady state thermal solution is solved and the thermal field is transferred to the mechanical solver where the 25 MPa pressure boundary condition on the inner surfaces of the header ports and the thermal strains are applied. The stress components along the SCLs are linearized following a straightforward procedure documented in ASME Section III, Division 5 [7]. The membrane stresses along every SCL must be less than the allowable stress for IN617 at the corresponding temperature, while the linearized stress (membrane + bending) must be less than 3 times the allowable stress in accordance with rules for analysis including secondary thermal stresses. If any of the 8 SCLs fail either of these criteria the analysis stops and zero cycles to failure is returned to indicate a faulty design for the given set of conditions and parameters. All of the cases run in the sensitivity analysis passed this test, however, and proceeded to the transient analysis. The transient thermal analysis is run using the average particle outlet temperature from the steady simulation as an isothermal initial condition. This assumes the heat exchanger does not flow sCO_2 during off-time and is sufficiently insulated. The sCO_2 flows at the full steady design condition at the first time step and the particle inlet temperature is linearly ramped up at the prescribed rate. In practice both the sCO_2 and particle flows would be ramped up and down, but for modelling simplicity both were turned on and off as a step function. The results then represent a limiting case where the system is thermally shocked at start up and ramp down. After the ramp up, the simulations are run for 30 minutes so that steady on-sun conditions are reached. The particle inlet temperature is then subsequently ramped back down at the same rate and run another 30 minutes. At this point, the sCO_2 flow is shut off and run for an hour to achieve the steady idle conditions. The transient stress history can now be obtained as shown in Fig. 4 for a case using nominal material properties and a ramp rate of 5°C/min. The average temperature along the SCL vs time is also plotted for two SCLs in Fig. 4.

A transient load check is performed to ensure that the linearized stresses do not peak to levels beyond the allowable or yield stress limits that could result in plastic failure. This condition never occurred within the limits of this parametric analysis, but a sufficiently fast ramp rate could theoretically cause a plastic failure to occur. The creep damage per cycle is next calculated by matching the transient stress history to experimental creep rupture test data. The ANL document relies on the creep-rupture tables provided in the BPVC code, but these were developed by applying extreme conservativism to various sources of raw tensile test data. This is necessary for ensuring safe designs of nuclear components, but this study aims to make more accurate lifetime predictions and thus implemented the raw experimental data. Larson-Miller parameter curves for the same experimental data were fitted by Messner et al. [8]. The creep data exhibits significant spread in cycles-to-failure at matched temperature and stress levels, so the authors provided the parameters for the mean and 95% lower and upper bounds. The ao term in their formulation, shown in Fig. 5, accounts for the experimental spread. The rupture time then varies with the max linearized stress and temperature levels along the various SCLs. Integrating the inverse of the rupture-time curve over one 24-hour cycle provides the creep damage fraction per cycle. To perform the integration, the daily cycle is assumed to consist of a 14-hour long on-sun time consisting of a ramp-up to steady state followed by a dwell period. The remaining 10 hours are idle time consisting of the ramp down time and hold at the cold particle outlet temperature. The ramp rate assigned defines the length of the ramp periods and the remaining time at steady on-sun and idle conditions. These cycle periods are labelled in the transient history plot in Fig. 4 for reference. The same document by Messner et al. developed fatigue life equations based on the material, temperature, and maximum strain range. The fatigue damage was predicted using their fit, however, it was found that the even for the most aggressive ramp rates, the strain ranges that emerge result in a negligible amount of fatigue damage, several orders of magnitude less than the creep damage. The creep damage is far more pronounced due to the elevated pressures

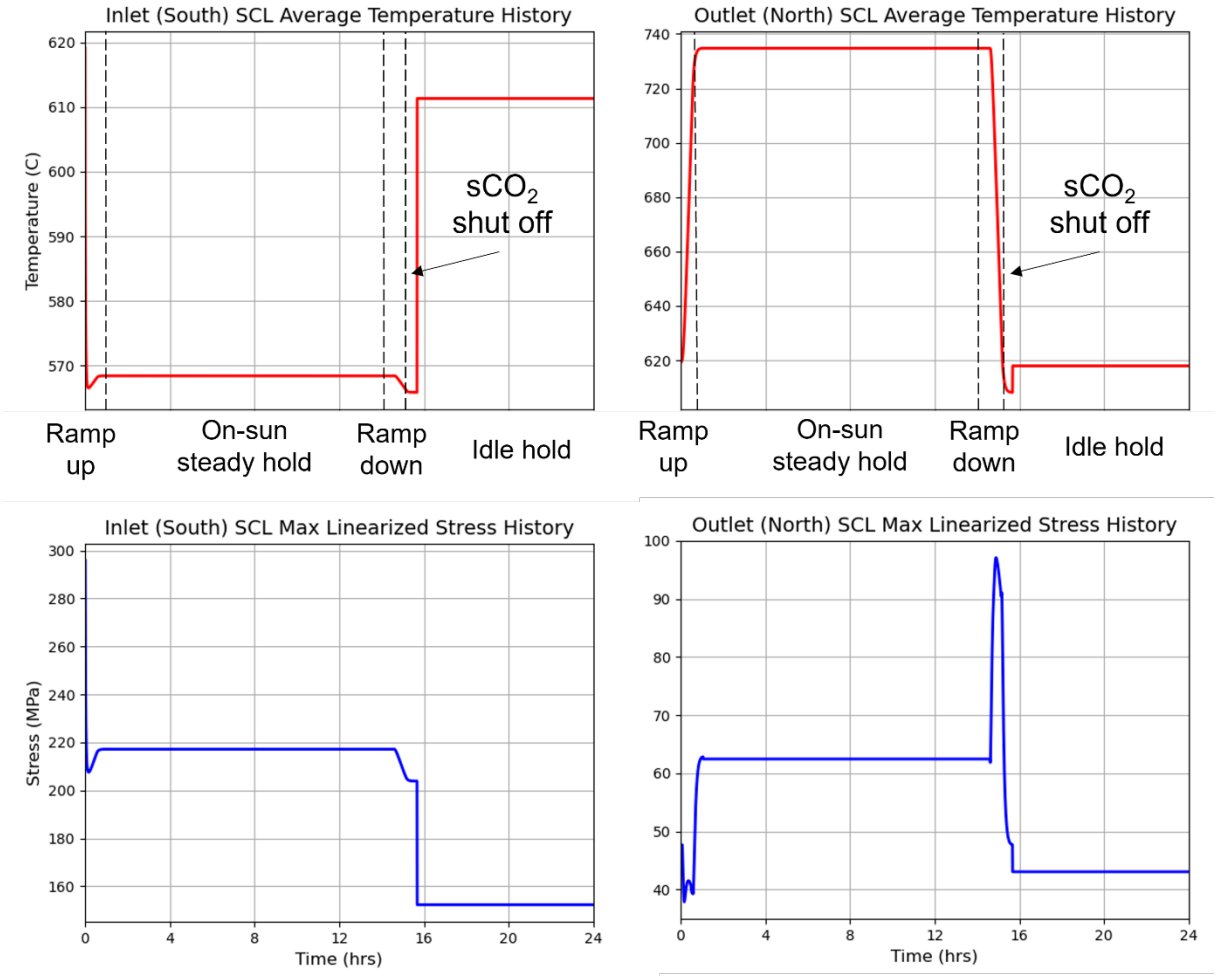

Figure 4. *Transient maximum linearized stress and average temperature histories for Outlet (North) and Inlet (South) SCLs using nominal material properties and 5°C/min ramp rate*

Materials	*Equations:* $t_r = f(T, \sigma)$	*Coefficients*	
		Average rupture	*95% prediction lower bound rupture*
Alloy 617	$10^{\left(\frac{a_1(log_{10}S)+a_0}{T+273.15} - C\right)}$	C = 13.22 a_1 = -4676.95 a_0 = 26779.12	C = 13.22 a_1 = -4677.52 a_0 = 25701.18

Figure 5. *IN617 time-to-rupture correlations (Messner et al. [8]) from Larson-Miller parameters fit to mean and 95% lower bound of experimental creep rupture test data*

and temperatures at G3P3 operating conditions. The approximate number of cycles-to-failure then can be evaluated simply by taking the inverse of the creep damage fraction per cycle without having to evaluate the creep and fatigue damage interaction.

4. Parametric Sensitivity Study

The sensitivity study is conducted by coupling Sandia's parametric analyses tool Dakota [9] to the SIERRA solvers. Seven independent variables are parameterized using a Latin hypercube sampling method. The ranges for each are provided in Table 2. The heat transfer coefficient between the sCO_2 and microchannels as predicted by the Gnielinski correlation along the advective bars is multiplied by a value between 0.75 and 1.25, representing ±25% uncertainty. The same scaler is applied to the temperature dependent function for the effective bed thermal

conductivity. The particle-to-wall gap conductance term is used in the thermal solver to simulate the additional near-wall thermal resistance due to voids in the contact layer. This value is critical to accurately predicting the overall heat transfer for heat exchangers using flowing packed particle beds as detailed by Adapa et al. [10] but is highly variable based on particle bed characteristics and design. A range of 1000-3000 $W\text{-}m^{-2}K^{-1}$ is used based on experimental measurements from Maskalunas et al. [11]. A wide range of ramp rates, 3 to 20 °C/min are queried. It is expected that for the mechanical behavior the elastic modulus (E) would be a sensitive parameter, so a mean room temperature value for wrought IN617 of 211 MPa is used and a ±25% uncertainty is arbitrarily applied to account for potential variations due to heat treatment and diffusion bonding processes. E remains temperature dependent with the same relative reduction with increasing temperature, only altering the room temperature baseline value. The fatigue cycles-to-failure calculation was based on the max strain range and used the IN617 curve fits by Messner et al. [8]. A relatively arbitrary range of 0.1 to 10 was applied to replicate the order of magnitude spread in the tensile fatigue test experimental data. A more sophisticated method could have been applied to capture the experimental variation, but it was expected that the fatigue damage would have an insignificant impact relative to creep for this application. The five aforementioned variables were parameterized using uniform distributions over their respective ranges of values. The sixth variable was the a_0 term which captures the experimental spread for IN617 creep tests. The upper and lower ranges shown in Table 2 came directly from the Messner et al. curves and define the 95% bounds under a normal distribution.

Table 2. *Parametric bounds for independent variables in sensitivity study*

Variable	Range	Type
sCO_2 heat transfer coefficient scaler	0.75 – 1.25	Uniform
Effective bed conductivity scaler	0.75 – 1.25	Uniform
Gap conductance coefficient	1000 – 3000 ($W\text{-}m^{-2}K^{-1}$)	Uniform
Elastic modulus	158 – 264 (MPa)	Uniform
Ramp rate	3 - 20 (°C/min)	Uniform
Fatigue cycles-to-fail scaler	0.1 - 10	Uniform
Creep lifetime a_0 term	26779 (mean), 539 (std dev)	Normal

Variance-based sensitivity analysis is used to compare the relative effect each independent variable has on the lifetime prediction. This method calculates Sobol indices which sum to unity, so each can be conceptualized as the percent contribution toward the variance in the output and a hierarchy of sensitivity can be deduced. Direct calculation of Sobol indices would require upwards of 10,000 model evaluations, which is impractical since each model evaluation requires four independent simulations and can take up to a day each running on 128 computational processes. An alternative is to use a model emulator such as polynomial chaos expansion (PCE) to essentially fit the model predictions to the input space. This requires orders of magnitude fewer model evaluations to reach a statistically converged emulator. Additionally, the variance-based decomposition can be performed analytically to produce Sobol indices. To achieve convergence using the PCE method, the number of evaluations was doubled until the Sobol indices converged. It was found that 128 simulations are sufficient to achieve converged values. Scatter plots mapping the resulting 128 lifetime predictions versus the independent variables are provided in Fig. 6. Above each plot, the main Sobol index is labeled.

The results indicate that only two of the variables, E and a_0 have any significant correlation to the cycles-to-failure prediction. The remaining variables have Sobol indices several orders of magnitude lower in comparison. The uncertainty in the a_0 term used in the creep damage formula is responsible for approximately 78% of the variance in the output. The only terms with

a significant interaction Sobol value of 0.112 are the a_o and E terms. The independent Sobol values of each represent the contribution to the variance if each were varied in isolation while the other variables were fixed. The interaction term accounts for the variance when both variables are changed simultaneously. The result that the uncertainty in the fatigue damage prediction has no impact is not particularly surprising, as it is expected at Gen3 pressures and temperatures that creep damage will be much more significant. It is notable however, that even at high ramp rates the strain ranges are not enough to make fatigue damage a relevant contributor. Due to the lack of significant sampling at the higher ramp rates, however, the authors would caution against concluding that CSP heat exchangers can be ramped at these aggressive rates safely. A similar study confined to these higher ramp rates would provide a more statistically significant dataset to develop those conclusions. Additionally, it is possible that plastic failure could occur due to the peak stresses along the SCLs, particularly at higher values of E, even though the alternating stresses are acceptable. The results suggest that the uncertainty in the thermal inputs to the model can be relatively large, up to 100% for the gap conductance, and still have no effect because the spread in the experimental creep failure data is overwhelming. One realization of the model can result in a failure prediction due to creep that spans many orders of magnitude.

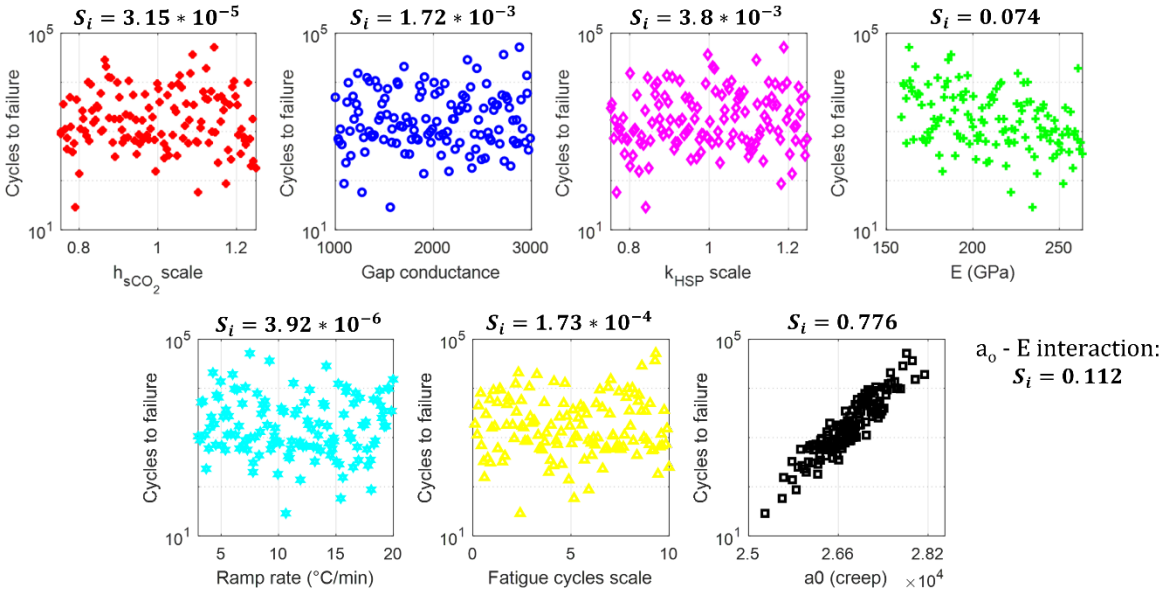

Figure 6. *Converged sensitivity study scatter plots*

5. Conclusions

This study presented a reduced order framework that significantly reduces the mesh size for a particle-sCO_2 heat exchanger model. The steady and transient thermomechanical response is well approximated when the microchannels are removed from the design and filled with solid material. The linearized stress values in the integral header ports compare reasonably with the full-featured model and allow comparable lifetime predictions to be made. The steady state stress values closer to the inner surface of the header ports and are slightly underpredicted on average because the interaction of the corner stresses at the microchannel exits are not captured. It is expected that these concentration stresses relax over time in practice and would do so in the fully featured model with application of a creep model in the FEA setup. The transient stresses therefore may be underpredicted, but the steady fields which account for most of the accumulated creep damage per cycle should be more accurate using this reduced order approach. The sensitivity study clearly demonstrates that uncertainty and lack of repeatability between wrought tensile specimen creep tests presents a major challenge when attempting to make accurate lifetime predictions. This unpredictability is a well-known phenomenon and

thought to be primarily caused by slight compositional variations between lots of wrought material as well as different heat treatments. Two identical creep tests performed on samples from the same lot are still subject to repeatability issues however because of inherent defects, sample preparation, and microstructural (grain size/arrangement) differences. To increase the predictive reliability of the model and allow for potential reduction on material overdesign and commensurate decreases in LCOE, a significant effort would be required to develop a creep database for diffusion bonded samples. The variation between specimen tests using matching diffusion bonding processes on wrought material from the same lot can be used to characterize the repeatability under best case conditions. A statistical analysis can be performed on tests from varying lots, where differences in heat treatment, preparation, composition, and microstructure are characterized carefully. This will not only give more geometrically specific creep damage formulations to implement in the model but may give insight into which variables correlate most strongly with the uncertainty. This could enhance the predictive ability whether through development of more sophisticated creep damage formulas, or through the inclusion of higher fidelity physics in the mechanical FEA model to capture the more deterministic elements.

Data availability statement

All computational simulations and results are available from the lead author upon reasonable request and approval of Sandia National Laboratories.

Author contributions

The lead author was responsible for all technical methodologies, investigations, and visualization. The second author served in a project administration and supervisory role along with technical review and editing.

Competing interests

The authors declare that they have no competing interests.

Funding

This work was funded in part or whole by the U.S. Department of Energy Solar Energy Technologies Office under Award Number 38474. This report was prepared as an account of work sponsored by an agency of the United States Government. Neither the United States Government nor any agency thereof, nor any of their employees, makes any warranty, express or implied, or assumes any legal liability or responsibility for the accuracy, completeness, or usefulness of any information, apparatus, product, or process disclosed, or represents that its use would not infringe privately owned rights. References herein to any specific commercial product, process, or service by trade name, trademark, manufacturer, or otherwise does not necessarily constitute or imply its endorsement, recommendation, or favoring by the United States Government or any agency thereof. The views and opinions of the authors expressed herein do not necessarily state or reflect those of the United States Government or any agency thereof. Sandia National Laboratories is a multimission laboratory managed and operated by National Technology & Engineering Solutions of Sandia, LLC, a wholly owned subsidiary of Honeywell International Inc., for the U.S. Department of Energy's National Nuclear Security Administration under contract DE-NA0003525.

Acknowledgement

The authors would like to thank Kevin Albrecht and Dereje Amogne at Vacuum Process Engineering for providing the commercial heat exchanger design drawings and operating conditions.

References

[1] C.P. Bowen and K.J. Albrecht, “Sensitivity Analysis of Moving Packed-Bed Heat Exchanger Models,” AIP Conf. Proc., 2815 (1): 030004, Oct 2023, doi: https://doi.org/10.1063/5.0148505.

[2] B. H. Mills, A.C Hetzler, and O.W. Deng, “Verification of Advective Bar Elements Implemented in the SIERRA/ARIA Thermal Response Code,” J. Verif. Valid. Uncert., 3(3): 031003, Sep 2018, https://doi.org/10.1115/1.4041837.

[3] V. Gnielinski, “New Equations for Heat and Mass Transfer in Turbulent Pipe and Channel Flow,” International Chemical Engineering, Vol. 16, No. 2, pp. 359-68, 1976.

[4] Sierra Thermal Fluid Development Team, 2021, “SIERRA Multimechanics Module: Aria Thermal Theory Manual—Version 5.0,” White Paper, Unlimited Release, Sandia National Laboratories, Albuquerque, NM, Report No. SAND2021-3922 695408.

[5] Sierra Thermal Fluid Development Team, “SIERRA Code Coupling Module: Arpeggio User Manual (V.5.10),” White Paper, Unlimited Release, Sandia National Laboratories, Albuquerque, NM, Report No. SAND2022-12441 709955.

[6] B. Barua, M. McMurtrey, R. Rupp, and M. Messner, “Design Guidance for High Temperature Concentrating Solar Power Components,” Argonne, IL (United States), Jan 2020, doi: 10.2172/1582656.

[7] ASME Boiler and Pressure Vessel Code Section III, 2021 Edition, “Rules for Construction of Nuclear Facility Components.”

[8] M.C. Messner and B. Barua, “A fast tool for receiver life estimation and design,” AIP Conf. Proc., 2445 (1): 020008, May 2022, https://doi.org/10.1063/5.0085669.

[9] B.M. Adams. et al. "Dakota, A Multilevel Parallel Object-Oriented Framework for Design Optimization, Parameter Estimation, Uncertainty Quantification, and Sensitivity Analysis: Version 6.14 User's Manual," Sandia Technical Report SAND2021-5822, May 2021.

[10] S.R., Adapa, X. Zhang, T. Feng, K.M. Chung, K.J. Albrecht, C.K. Ho, D.A. Madden and R. Chen, “Thermophysical Properties and Heat Transfer Coefficients for Flowing Packed Particle Beds,” arXiv preprint arXiv:2403.19892, Mar. 2024, https://doi.org/10.48550/arXiv.2403.19892.

[11] J. Maskalunas, G. Nellis, and M. Anderson, “The Heat Transfer Coefficient Associated with a Moving Packed Bed of Silica Particles Flowing through Parallel Plates,” Sol. Energy, 234, pp. 294–303, 2022, https://doi.org/10.1016/j.solener.2022.01.052.